J Mater Sci (2008) 43:5157–5167
DOI 10.1007/s10853-008-2722-y

Design of graded two-phase microstructures for tailored elasticity gradients

Shiwei Zhou · Qing Li

Received: 24 January 2008 / Accepted: 12 May 2008 / Published online: 7 June 2008

Abstract Being one of new generation of composites, functionally graded materials (FGMs) possess gradually changed physical properties due to their compositional and/or microstructural gradients. In literature, exhaustive studies have been carried out in compositional modeling and design, while limited reports are available for microstructural optimization. This article presents an inverse homogenization method for the design of two-phase (solid/void) FGM microstructures, whose periodic base cells (PBCs) vary in a direction parallel to the property gradient but periodically repeat themselves in the perpendicular direction. The effective elasticity tensor at each PBC is estimated in terms of the homogenization theory. The overall difference between the effective tensor and their target is minimized by seeking for an optimal PBC material topology. To preserve the connectivity between adjacent PBCs, three methods, namely connective constraint, pseudo load, and unified formulation with nonlinear diffusion are proposed herein. A number of two-dimensional examples possessing graded volume fraction and Young's modulus but constant positive or negative Poisson's ratios are presented to demonstrate this computational design procedure.

Introduction

Functionally graded materials (FGMs) are characterized by gradually changed physical properties due to a gradient (elevated) distribution of compositions and/or microstructures. The concept of FGM was proposed around mid-1980s [1] when the researchers in aeronautics and advanced materials attempted to seek desirable thermal properties, specifically, an insulative outer shell and conductive inner core, for soaring spacecraft suffering ultra high temperature gradient. Since then, rapid and significant progress has been made in both the fabrication and application of FGMs [2, 3].

Perhaps, the most amazing FGMs are not produced by human but by nature. Indeed, a large number of biological systems ranging from bones, sea shells to plant stems are composed of "optimally" graded microstructures, which have evolved over millions of years to accommodate the natural environment that they expose [2]. Of all these natural FGMs, the stems of bamboos have attracted substantial attention for their superior performance in resisting high external loading with a relatively light weight [4–7]. Bamboo is longitudinally reinforced by strong fibers proportionally distributed along the distance to the center of hollow stems. Experiments showed that the fracture toughness of such structures is even higher than some aluminum alloys [4]. It should be noted that one of the most important features of the natural FGMs like bamboo and bone is their self-optimized capability through modeling and remodeling their microstructures under certain level of mechanical stimuli [5].

It has been a fact of matter that engineers can develop new materials by morphologically mimicking natural FGMs. However, is it possible to invent ingenious materials which nature does not have or the mankind has not known yet? Since the microstructures of biological FGMs can be viewed as a result of an optimization through evolution and/or remodeling [5], it is worthwhile attempting to design new FGM microstructures by using the state-of-the-art topology optimization techniques [8]. Although classic topology optimization procedures were originally developed for

S. Zhou · Q. Li (✉)
School of Aerospace, Mechanical and Mechatronic Engineering, The University of Sydney, Sydney, NSW 2006, Australia
e-mail: Q.Li@usyd.edu.au

designing the stiffest structures, they have been successfully extended to the design of periodic composites composed of spatially repeated representative volume elements (RVEs) or periodic base cells (PBCs) in the last decade [9, 10].

To deal with the design of periodic composites, there are two relevant computational problems. On the one hand, the effective (or bulk) physical properties at a specific point (i.e., pixel for 2D or voxel for 3D) in the composite can be determined by using the homogenization procedure for a given material composition and microstructure [11, 12]. On the other hand, material compositions and microstructures can be sought by minimizing the difference between the homogenized effective properties and their target values. Being a relatively new computational technique, the latter, namely inverse homogenization, signifies a novel material design paradigm. It has enabled us to devise a range of new composite materials with extraordinary physical properties, e.g., negative thermal expansion coefficient (i.e., expansion when cooled while shrinkage when heated) [13], extremal conductivity [14, 15], maximum permeability [16], etc. Recently, with the mature of fabrication techniques like selective laser melting (SLM) [17], especially the advent of solid freeform fabrication (SFF) technologies (e.g., three-dimensional printing [18, 19]), it has become possible to fabricate various complicated microstructures in a fashion of point by point and layer by layer directly from a computer model. An obvious benefit of such fabrication technology is that it allows more sophisticated computational design of FGM from not only compositional but also microstructural aspects. In particular, the microstructural details can be properly reflected by directly printing them into 3D part with an acceptable microscopic resolution. A seamless integration of the inverse homogenization with SFF has been reported in [20–22] for designing and fabricating porous tissue scaffolds. This technology has provided us with considerable flexibility to develop more demanding FGM microstructures being of desirable property gradients.

However, the existing version of inverse homogenization procedure has mainly focused on generating homogeneous periodic composites without purposely involving graded effective physical properties, where all the base cells are identical in their composition and architecture. To model inhomogeneous media, some attempts are made in incorporating the inverse homogenization into base cell design. Lin et al. [20, 21] developed a two-stage method for fusion cage design, where global material layout and local microstructures are optimized in a serial fashion. The spatial volume fraction and elasticity tensor generated from the global design were used as a goal for the topological design of local base cells. As a result, an inhomogeneous tissue scaffold is obtained with non-uniform mechanical properties that match to the property gradient of native spinal bone tissues. Chen and his coworkers [23, 24] as well as Seepersad et al. [25] considered non-identical base cells for modeling inhomogeneous media, where the size and volume fraction of base cells are the variables for graded properties. However, these studies mainly account for the same or similar microstructural topology, and largely rely on the design of individual base cell without intentionally considering their interconnection.

From macroscopic design perspective, pattern repetition [26] is another technique that allows one master and a number of slave structural components to have similar topological layouts whereas keep the connectivity, where each component has its own coordinate system with different scale factors in the demand of the size difference between the components. This method has been successfully used by Altair Company to design the ribs in a wing model and other products subjected to manufacturing constraints. It might be possible to apply this method to the microstructural design of FGM as it can guarantee two of the most important features, namely the connectivity and similarity between adjacent base cells. However, great effort is still needed to address the issues like mapping from macro to micro scales, and associative calculation of effective physical properties.

This article attempts to expand such an individual PBC design methodology in two different ways on (1) systematically addressing the connectivity issues between different PBCs and (2) formulating the design of microstructure gradient in a graded base cell (GBC) model to accommodate desirable property gradation in a *unified* formulation. Accordingly, three different techniques are presented below to tackle the connectivity issue in the PBC design. These techniques will be demonstrated through a number of illustrative examples, which could be precisely fabricated by using SFF technologies in the future.

Materials and methods

To develop graded microstructure for a specific FGM, two different approaches may be applied on either designing PBC representing a pixel/voxel in different FGM depths *individually* or formulating the property gradient across a limited number of PBCs *as a whole*. For the former, we first generate the local microstructures in different PBCs, separately, and then assemble all the PBCs to form FGM structure. For the latter, the graded microstructures across all the PBCs (namely GBC) are generated altogether in a unified formulation. In both the cases, the effective properties are estimated by using the finite element (FE) based homogenization procedure [11, 12, 27]. The differences between the effective values estimated from the homogenization and desired property values are minimized by

seeking for an ideal microstructural topology in either PBC or GBC models [10, 28].

Both the PBC and GBC microstructures in this article are represented in a density-based model, where the volume fraction of solid material at point (element) $\mathbf{x}$, also denoted in relative density $\rho(\mathbf{x})$, serves as the design variables. Taking a two-phase (solid-void) media as an example, the void and solid phases are represented by $\rho(\mathbf{x}) = 0$ and $\rho(\mathbf{x}) = 1$, respectively. Nevertheless, intermediate density, i.e., $0 < \rho(\mathbf{x}) < 1$, is allowed during design in order to relax the original ill-posed topology optimization problem [29].

It should be noted that FGMs are generally expected to have a continuum distribution of their constituent phases and corresponding properties, whose volume fractions are usually depicted by continuous concave upward or concave downward functions along gradation direction [30]. Nevertheless, a class of FGMs has been fabricated by bonding different compositional layers or connecting cellular microstructures together, in which the continuity of property gradients can only be approximated in a finite number of discontinuous layers or cells [30]. In fact, the microstructures of many natural FGMs like cancellous bones and bamboo stems are composed of such a layer-by-layer or cell-by-cell manner. From this perspective, the layer- or cell-wise representation of material distribution is compatible with the base-cell design model, in which each base cell represents part of one layer or one pixel/voxel in FGM. The discrete design variable, namely the volume fraction of candidate phase at each FE, can approximately reflect the local composition of each particle of FGM constituent.

Inverse homogenization method

In traditional FGM design, the local effective properties are often evaluated by Mori–Tanaka [31] or the self-consistent [32] methods. Both of them only rely on local volume fractions and the properties of matrix and inclusion phases without consideration of the microstructures. It was found that the applicability of these two methods is dependent upon some conditions [33]. For example, when FGM constitutes well-defined continuous matrix (i.e., the first phase) and discontinuous inclusion (the second phase), the local properties for FGM is better interpolated by the Mori–Tanaka method. The self-consistent method is more suitable for the FGM with a skeletal microstructure in a wide transition zone between distanced matrix phases. It was also reported in [33] that the Mori–Tanaka estimate coincides with the Hashin–Shtrikman bounds [34] when the two candidate phases have a greater modulus difference. Actually, based upon the inverse homogenization method [15, 35], we found exact microstructures for two-phase composites whose local thermal conductivity can reach the lower/upper Hashin–Shtrikman bounds, depending on whether insulative or conductive phase serves as the matrix [15, 35]. In this article, for each layer of the FGM, the local properties are integrated over the RVE in terms of the homogenization method [11, 12, 27].

The typical homogenization theory [11, 12, 27] may not exactly be applicable to FGM base cells because of non-periodicity in the gradient direction. This implies that the effective values calculated via the homogenization algorithm may not be exactly correct. However, an adequate accuracy can be achieved if the size of base cells is relatively small compared to the property gradient. In other words, if the change (descent or ascent) in the effective properties across each base cell is sufficiently small, the homogenized values can practically approximate to the true values of the FGM properties. In this respect, existing fabrication technologies allow less than 1–5 μm geometric features [22], making such an approximation practically sensible.

According to the homogenization theory [11, 12, 27], the effective elasticity tensor for a microstructure occupying domain Ω is given by

$$\bar{G}_{ijkl}(\rho) = \frac{1}{|\Omega|}\int_{\Omega} D_{ijmn}(\rho)\left(\bar{\varepsilon}^{kl}_{mn} - \tilde{\varepsilon}^{kl}_{mn}\right) \mathrm{d}\Omega \tag{1}$$

where $|\Omega|$ denotes the area (or volume in 3D) of the design domain Ω. The four linearly independent unit test strain fields $\bar{\varepsilon}^{kl}_{mn}$ are given as $\bar{\varepsilon}^{11}_{mn} = (1\ \ 0\ \ 0\ \ 0)^{\mathrm{T}}$, $\bar{\varepsilon}^{22}_{mn} = (0\ \ 1\ \ 0\ \ 0)^{\mathrm{T}}$, $\bar{\varepsilon}^{12}_{mn} = (0\ \ 0\ \ 1\ \ 0)^{\mathrm{T}}$ and $\bar{\varepsilon}^{21}_{mn} = (0\ \ 0\ \ 0\ \ 1)^{\mathrm{T}}$, respectively in 2D cases. The strain fields $\tilde{\varepsilon}^{kl}_{mn}$, induced by the test strains, are the solutions to the following equation

$$\int_{\Omega} D_{ijmn}\varepsilon_{ij}(v)\tilde{\varepsilon}^{kl}_{mn}\,\mathrm{d}\Omega = \int_{\Omega} D_{ijmn}\varepsilon_{ij}(v)\bar{\varepsilon}^{kl}_{mn}\,\mathrm{d}\Omega \tag{2}$$

where the virtual displacement field $v \in H_{\mathrm{per}}$ belongs to the periodic Sobolev functional space.

The local elasticity tensor is denoted as $D_{ijmn}(\rho)$, which can be simplified in a matrix form for 2D isotropic materials, given by

$$G_{ij}(\rho) = \begin{bmatrix} D_{1111} & D_{1122} & 0 \\ D_{1122} & D_{2222} & 0 \\ 0 & 0 & D_{1212} \end{bmatrix} = \frac{E(\rho)}{1-\upsilon^2}\begin{bmatrix} 1 & \upsilon & 0 \\ \upsilon & 1 & 0 \\ 0 & 0 & 0.5(1-\upsilon) \end{bmatrix} \tag{3}$$

where υ denotes Poisson's ratio and $E(\rho)$ is the density-related Young's modulus, usually interpolated as

$$E(\rho) = \rho^p E_1 + (1-\rho)^p E_2 \tag{4}$$

in terms of the "solid isotropic material with penalization" (SIMP) model in topology optimization [36]. The Young's moduli for the solid and void phases are denoted by E_1 and E_2 respectively. In order to avoid computing singularity, E_2

is usually set as a very small positive value other than 0 (e.g., $E_2 = 10^{-3}E_1$). The penalty factor p in the SIMP interpolation should be chosen properly to ensure the bulk modulus not higher than the upper Hashin–Strikman (HS) bound [34]. In addition to Eq. 4, the local Young's modulus can also be interpreted by the following scheme as proposed by Stolpe and Svanberg in [37], given by

$$E(\rho) = E_2 + \frac{\rho(E_1 - E_2)}{1 + q(1-\rho)} \tag{5}$$

For the maximal stiffness problem, Stolpe and Svanberg proved that the objective function (mean compliance) is concave for a priori known penalty factor $q \geq (E_1 - E_2)/E_1$, thus the problem is of a global optimum. In addition to the aforementioned interpolation schemes, Bendsøe and Sigmund [38] also directly used the upper HS bound as the interpolation scheme for the problems of the maximal stiffness and generated desirable black/white results. The work in [15, 35] further indicates that the HS bound-based interpolation is self-weighted for the composite design with the extremal thermal conductivities where no penalty factors are needed.

Mathematically, the inverse homogenization can be formulated as the least square of the difference between the entries of the target $\overset{*}{G}$ and the homogenized effective elastic tensor $\bar{G}$, as

$$\min_{\rho} J(\rho) = \sum_{i,j=1}^{3} r_{ij}\left(\overset{*}{G}_{ij} - \bar{G}_{ij}\right)^2 \tag{6}$$

where r_{ij} are positive weighting factors used to emphasize the role of different entries in the objective function. The value in Eq. 6 can be regarded as a potential energy as it evaluates how different the effective elasticity is from its target.

In order to employ the MMA method [39] for the minimization of Eq. 6, the sensitivity of the objective is evaluated as,

$$\frac{\partial J}{\partial \rho} = -2\sum_{i,j=1}^{3} r_{ij}\left(\overset{*}{G}_{ij} - \bar{G}_{ij}\right)\frac{\partial \bar{G}_{ij}}{\partial \rho} \tag{7}$$

where $\partial \bar{G}_{ij}/\partial \rho$ can be derived from the adjoint variable method [40], as

$$\frac{\partial}{\partial \rho}\bar{G}_{ij}(\rho) = \frac{1}{|\Omega|}\int_{\Omega}\left(\bar{\varepsilon}^{ii}_{ii} - \tilde{\varepsilon}^{ii}_{ii}\right)\frac{\partial G_{ij}(\rho)}{\partial \rho}\left(\bar{\varepsilon}^{jj}_{jj} - \tilde{\varepsilon}^{jj}_{jj}\right)\mathrm{d}\Omega \tag{8}$$

Connectivity between PBCs

In a typical homogeneous periodic composite, all the boundary conditions of a base cell are imposed periodically so that the same effective (bulk) material properties can be attained at any point of the composite. Due to the nature of periodicity, there is generally no connection problem between adjacent PBCs. In inhomogeneous FGM, however, one of the bi-directional (2D) or tri-directional (3D) periodicity must be released to accommodate a property gradient along this direction. Thus, ensuring proper connectivity between adjacent PBCs becomes a significant issue confronting in FGM design. To tackle this problem, three different methods, namely (1) connective constraints, (2) pseudo load, and (3) unified formulation with nonlinear diffusion, are proposed in this article as follows.

Kinematical connective constraint (KC) method

Since there is no guarantee for a proper boundary connection along gradient direction, one of the simplest methods is to impose connective constraints in the boundary across the graded PBCs. As illustrated in Fig. 1 for a FGM having *NL* layers, the yellow (grey in black/white pictures) areas in the gradient boundary are permanently occupied by solid materials, serving as imposed connective regions to enforce continuous edge-to-edge bonds between the adjacent PBCs. To make the homogenization more closely approximate the effective elastic tensor, the number, location, and size of the connectors in gradient direction should be as identical as possible, yielding a mostly possible periodic boundary condition in gradient direction. Obviously, imposing such a "non-design connector domain" in PBC model may be a critical step since it can lead to different final topologies. As a reference, one can generate a PBC design based on the typical periodic boundaries for a desired property and then follow the topology to prescribe a more suitable connective zone in the non-PBC boundaries. Taking FGM with the extremely positive Poisson's ratio as an example, the four corners should not be set as the connective zones as the commonly known optimal structure in a shape of hexagon [10, 28] has no solid materials close to the corners.

Pseudo load (PL) method

It is a fact of matter that the connectivity between PBCs enables the FGM to sustain external loading with certain stiffness. For this reason, one can impose the base cell a

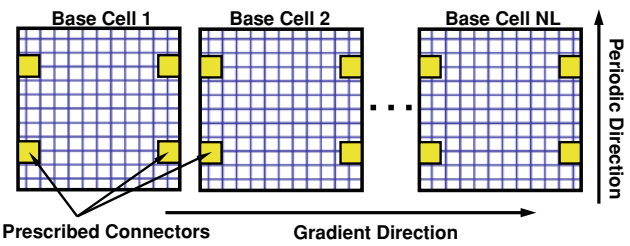

Fig. 1 Kinematical connective constraints between periodic base cells

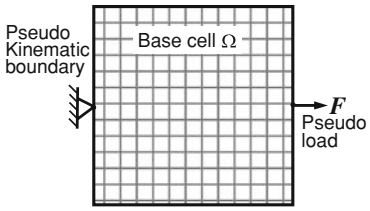

Fig. 2 Pseudo load and boundary condition in PBC

pseudo load and a kinematic boundary in the gradient boundaries, as illustrated in Fig. 2. The way to define the pseudo load and kinematical boundary condition should follow the strategies given in Fig. 1, i.e., preserving periodic boundary conditions whenever possible. Thus the load and kinematical boundary conditions are prescribed in the opposite PBC gradient boundaries identically for all PBCs (Fig. 2). This treatment allows a pseudo stiffness criterion to be included in the design objective, in a compliance term, as,

$$\min_{\rho} J(\rho) = \sum_{i,j=1}^{3} r_{ij}\left(\overset{*}{G}_{ij} - \bar{G}_{ij}\right)^2 + \eta \int_{\Omega} \varepsilon(u) D(\rho) \varepsilon(u)\, \mathrm{d}\Omega \tag{9}$$

where the strain and displacement induced are denoted as ε and u, respectively. Ω represents the domain of base cell as in Fig. 2. The weighting factor η should be sufficiently small; otherwise the mean compliance term could play an overly dominant role in the design. The introduction of kinematical boundary and pseudo load in the gradient boundaries usually lead to proper connective zones being formed in final PBC. Although the compliance (the 2nd term) is relatively small compared to the potential energy (the 1st term) in the objective function (to be shown in the example), it acts as the seeds in the PBC design, where the solid material grows around the pseudo boundary and loading areas, thus capable of connecting the PBCs across the graded boundaries.

Unified formulation (UF) with nonlinear diffusion method

The aforementioned two approaches are proposed to tackle the connectivity issue from individual design of PBCs at different gradient depths. To achieve a certain property gradient, it appears more meaningful to design graded FGM microstructures as a whole, where the connectivity between PBCs can be considered altogether through a unified formulation. Our previous studies demonstrated that the nonlinear diffusion [41, 42] is of considerable significance in suppressing checkerboard patterns and blurred boundaries for the PBC design [14, 15], thereby ensuring proper topological interconnection. Theoretically, the large norm of density gradient occurs in the area whose solid phase is being broken. Thus the minimization of the norm of the density gradient can effectively avoid the occurrence of disconnectivity between PBCs. For this reason, the design problem is formulated in terms of the least square of property differences, nonlinear diffusion energy and compliance, as

$$\begin{aligned}\min_{\rho} J(\rho) = &\sum_{k}^{NL}\sum_{i,j=1}^{3} r_{ij}^{k}\left(\overset{*}{G}{}_{ij}^{k} - \bar{G}_{ij}^{k}\right)^2 + \tau^2 \int_{\widehat{\Omega}} \varphi\left(\|\nabla\rho\|\right) d\widehat{\Omega} \\ &+ \eta \sum_{k}^{NL} \int_{\Omega} \varepsilon(u) D(\rho) \varepsilon(u)\, d\Omega \end{aligned} \tag{10}$$

where τ is a weighting factor for the diffusion energy.

The objective function in Eq. 10 is actually a generalized form for all these three different methods proposed for the FGM design in this article. For example, in the first (KC) and third (UF) methods, the weight η may be set to zero to omit the compliance requirement, whereas the prescription of kinematical connective constraints is no longer required in the last two (i.e., PL and UF) methods. Nevertheless, the nonlinear diffusion terms can be included for all the three methods to play a role on suppressing checkerboard patterns and obtaining edge-preserving topologies.

It is noted that in the first two (KC and PL) methods, the effective domain of nonlinear diffusion term $\widehat{\Omega}$ in Eq. 10 is the same as PBC Ω, whereas in the last (UF) method, the effective domain $\widehat{\Omega}$ equals the summation of all PBCs within GBC so that the nonlinear diffusion takes effect in all different layers altogether.

The sensitivity of the diffusion energy with respect to the density is given by

$$\frac{\partial\varphi(\|\nabla\rho\|)}{\partial\rho} = -\mathrm{div}\left[\frac{\partial\varphi}{\partial(\|\nabla\rho\|)}\frac{1}{\|\nabla\rho\|}\nabla\rho\right] \tag{11}$$

where div denotes the divergence of a vector. Derived from Fick's law and the continuity condition, the diffusion process was firstly used to describe mass transport. Different diffusion functions determine different diffusion processes. For example, if $\varphi(\|\nabla\rho\|) = \frac{1}{2}\|\nabla\rho\|^2$, the right part of Eq. 11 degenerates to the well-known Laplace operator, which coincides with the linear filter models in topology optimization [43]. More details about the requirements of diffusion functions are described in [41]. In the FGM design, blurred edge with ambiguity in interpreting phase interfaces can be effectively avoided by including the nonlinear diffusion term in Eq. 10.

The computational design process of FGM can be depicted in a detailed flowchart as Fig. 3. These three methods of reinforcing connectivity can be reflected in PBC/GBC modelling and/or design objective function. One may attempt all these methods to generate different solutions for comparison.

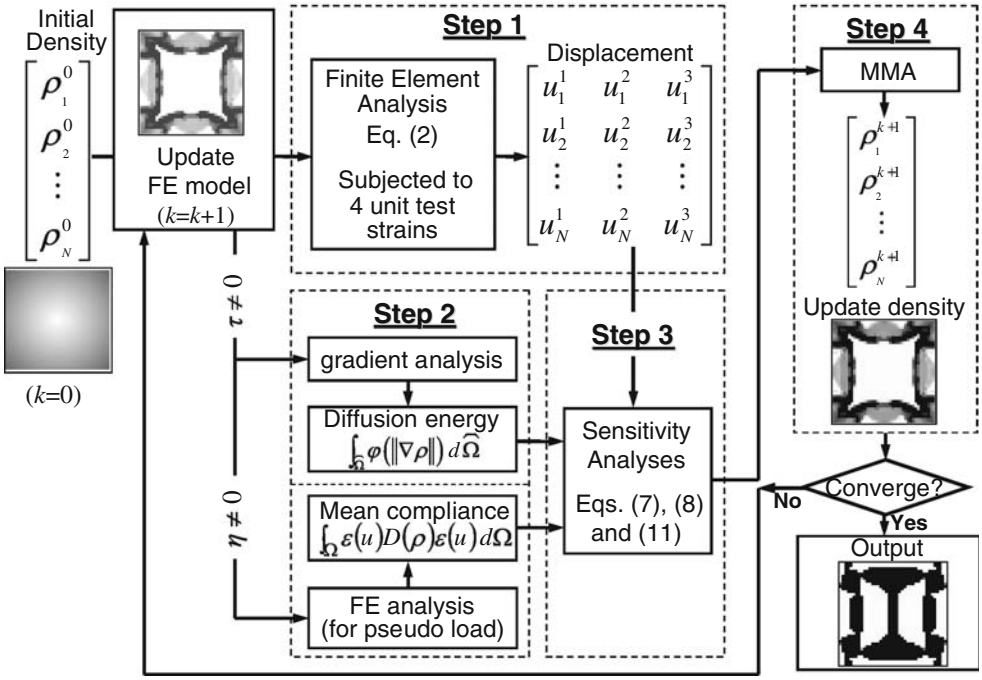

Fig. 3 Flowchart of the design process

It should be pointed out that the present inverse homogenization is established for a mono-directional property gradient. Mathematically it may not be applicable to bi- (2D) or tri-directional (3D) situations because there is no longer any base cell periodicity in such cases. However, if the property gradient is sufficiently small compared to the size of base cell, a quasi-periodicity could be considered. As a result, the FGM microstructures can still be designed by using the inverse homogenization method presented, as long as the connectivity between PBCs can be maintained.

Results and discussion

It is assumed that the solid phase represented by dark color in all the examples below has a unity Young's modulus of $E_1 = 1$ and a Poisson's ratio of $\upsilon = 0.3$. Using such a basis material, we seek for FGMs with certain graded Young's modulus and volume fraction through a limited number of layers (12 layers in all the examples below). Meanwhile, their effective Poisson's ratios are amounted to either a positive constant value of $\upsilon = 0.9$ or a negative constant value of $\upsilon = -0.85$. To show the FGM microstructures, each layer in the following examples is made up by three periodically repeated PBCs. For clarification, the GBCs in the middle row are highlighted by the dashed line.

In the PBC topology optimization, two initial values of material distributions are typically adopted in literature [9, 10, 15]. Initial Design 1 involves a material distribution, where the pixel/voxel (elemental) density (or volume fraction) is proportional to the distance from the pixel center to the PBC center (as shown in Fig. 4a). Initial Design 2 involves a pattern whose elemental density is inversely proportional to this distance (as shown in Fig. 4b). The color bar on the top of Fig. 4 indicates the relation of the grey-scaled pixel to the value of volume fraction. For the former, the high-density materials extend from boundary to the core area in the radial direction. One benefit of using Initial Design 1 is that the connectivity between adjacent PBCs may be better than that generated from Initial Design 2 since initial solid materials in the boundaries may not be removed completely during design, thereby remaining certain degree of connectivity. For the latter, the connectivity may not be guaranteed and one of the aforementioned methods be often needed. Nevertheless, such an initial design can yield different FGM microstructures, sometimes more beneficial to design and fabrication.

In the following examples, all the design parameters are summarized in Table 1, in which the target elastic tensor at the kth layer is denoted by $G^k = \beta^k G^+$ or $G^k = \beta^k G^-$ with positive or negative Poisson's ratio, respectively, where

$$G^+ = \begin{bmatrix} 1 & 1 & 0 \\ 1 & 1 & 0 \\ 0 & 0 & 0 \end{bmatrix} \quad \text{and} \quad G^- = \begin{bmatrix} 1 & -0.85 & 0 \\ -0.85 & 1 & 0 \\ 0 & 0 & 0.2 \end{bmatrix}.$$

Example with kinematical connective constraint (KC)

Example 1 is used to show the connective constraint method, where the yellow (grey in black/white pictures) regions in all

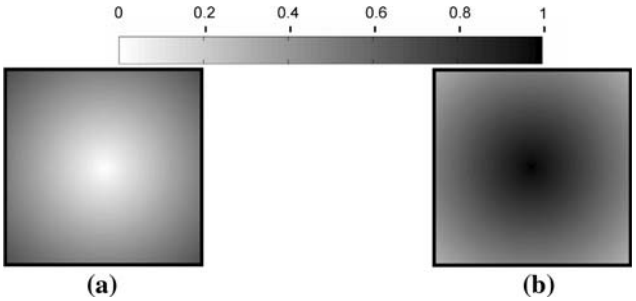

Fig. 4 Initial microstructures: (a) Initial Design 1; (b) Initial Design 2

these 12 PBCs are the fixed non-design domains as in Fig. 5. The interpolation scheme for local Young's modulus is based on Eq. 5 with $q = 5$. Starting from Initial Design 1, we can first obtain the optimized microstructure for each of the 12 PBCs, and then assemble such 12 individual PBCs to form the FGM configuration shown in the bottom of Fig. 5. In this example, the Young's modulus varies from 0.0058 (left) to 0.0373 (right) across these 12 layers, and correspondingly, the volume fractions change from 0.2516 to 0.4823 through the layers, as plotted in the top of Fig. 5. The effective Poisson's ratio of this FGM is maintained in a desirable positive constant of $\upsilon = 0.90$. In this example, it is observed that the microstructural topology is identical in the different layers of PBCs.

Example with pseudo load (PL)

In the PBC models of Example 2, two fixed points on the left edge are prescribed as the pseudo kinematical boundaries and other two corresponding positions on the right edge are assigned two pseudo point forces (Fig. 6a), which yields the microstructural topology as in Fig. 6b). Figure 7 shows the assembly of the FGM, in which the Young's modulus grades from 0.0453 (left) to 0.1516 (right), and correspondingly, the volume fraction varies from 0.4057 to 0.6914 across these PBC layers (top of Fig. 7). In this example, a negative effective Poisson's ratio around $\upsilon = -0.51$ is attained for all the PBCs. The convergence of the objective function and its individual components for the fifth layer of PBC (i.e., Fig. 6b) are plotted in Fig. 8 with a logarithmic scale. It is observed that although the diffusion energy and mean compliance only make up a small portion of the total objective energy, the introduction of them allows automatically designating proper connection between PBCs. It should be pointed out that in this example, Initial Design 2 was adopted, where if there were no pseudo loads and boundary prescribed, material breakage between PBCs could have been observed. It is also seen that although the PBC topologies differ considerably from Layer 1 to Layer 12 due to their individual designs, all the PBC connectivity preserved well.

Table 1 Design parameters for demonstrative examples

	Example 1	Example 2	Example 3	Example 4	Example 5
MC	KC	PL	UF	UF	UF
ID	1	2	1	2	2
Mesh	40 × 40	40 × 40	50 × 50	50 × 50	30 × 30
τ_{n+1}	$\tau_{n+1}^2 = 0.98\tau_n^2$	$\tau_{n+1}^2 = 0.99\tau_n^2$	$\tau_{n+1}^2 = 0.99\tau_n^2$	$\tau_{n+1}^2 = 0.98\tau_n^2$	$\tau_{n+1}^2 = 0.96\tau_n^2$
τ_0	0.01	0.005	0.06	0.025	0.04
η	0	0.02	0	0	0
$\beta_i G^0$	$\beta_i G^+$	$\beta_i G^-$	$\beta_i G^+$	$\beta_i G^+$	$\beta_i G^-$
β^1	0.040	0.065	0.035	0.035	0.08
β^2	0.055	0.070	0.040	0.040	0.10
β^3	0.060	0.085	0.045	0.045	0.12
β^4	0.065	0.090	0.050	0.050	0.14
β^5	0.070	0.110	0.055	0.055	0.16
β^6	0.075	0.145	0.060	0.060	0.18
β^7	0.080	0.150	0.065	0.065	0.20
β^8	0.085	0.160	0.070	0.070	0.22
β^9	0.090	0.170	0.075	0.075	0.24
β^{10}	0.095	0.190	0.080	0.080	0.26
β^{11}	0.100	0.205	0.085	0.085	0.28
β^{12}	0.105	0.210	0.090	0.090	0.30

Note: MC, the "methods for connectivity constraint"; ID, initial design

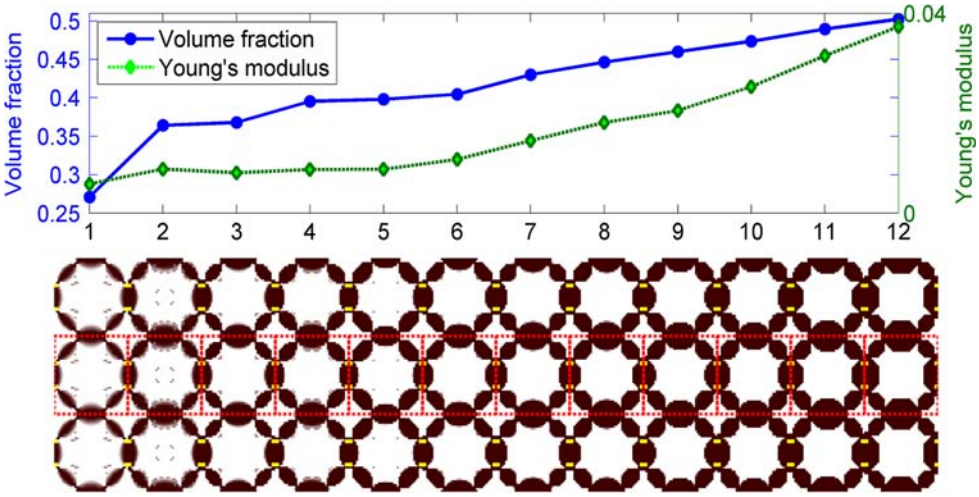

Fig. 5 FGM with positive Poisson's ratio of $\upsilon = 0.90$ (Example 1)

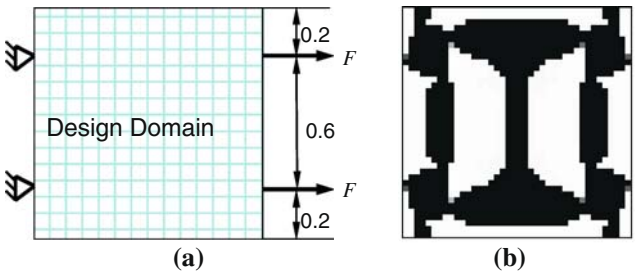

Fig. 6 PBC model and design result with pseudo load: (**a**) model with two point loads and fixed kinematical boundary and (**b**) optimal result for the 5th layer of FGM

Examples in a unified formulation with nonlinear diffusion (UF)

Unlike the aforementioned examples, where the base cells are designed individually, the examples in this section are based upon the unified formulation designs in a 12-layer GBC model. The nonlinear diffusion takes effect in the entire GBC design domain for ensuring connectivity between these 12 layers of PBCs. As such, the inverse homogenization is carried out over all layers of PBCs altogether as they are regarded as an integral structure rather than independent cells. Note that in this example, Initial Design 1 (Fig. 4a) is repetitively set up as the seeds of 12 base cells within GBC domain. The homogenization is also carried out according to each of such seeded base cells. As in Fig. 9, the microstructure in Example 3 demonstrates a desired role of the nonlinear diffusion on improving PBC connectivity. The effective Poisson's ratio of this FGM reaches an acceptable positive value of $\upsilon = 0.89$, whereas the Young's modulus and volume fraction vary from 0.0096 to 0.0238 and from 0.1736 to 0.3772, respectively, across all the 12 PBC layers from left to right (as in the top of Fig. 9). It is particularly worth noting that although the resulting topologies are different in different PBC layers, they connect with each other seamlessly.

Example 4 is presented in Fig. 10, whose microstructure is generated from Initial Design 2 (Fig. 4b) seeded in a 12-layer GBC model. The top subfigure in Fig. 10 illustrates

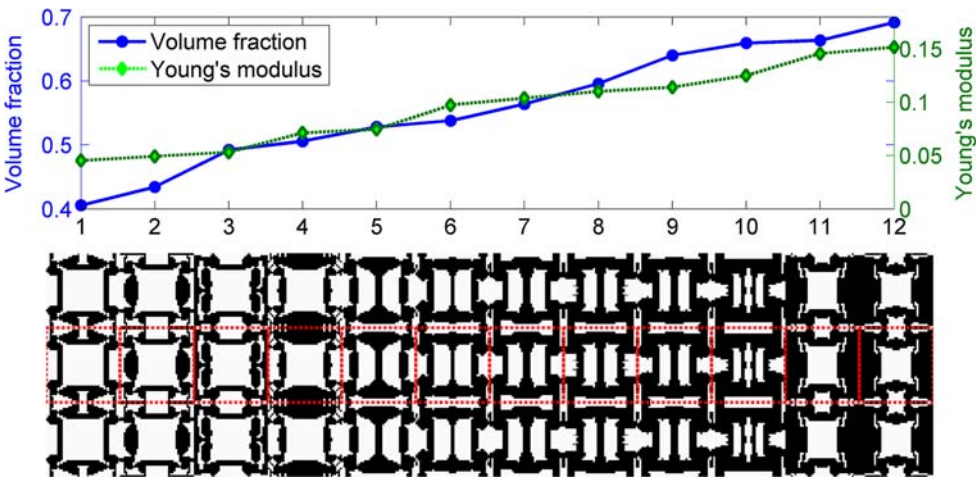

Fig. 7 FGM with negative Poisson's ratio $\upsilon = -0.51$ (Example 2)

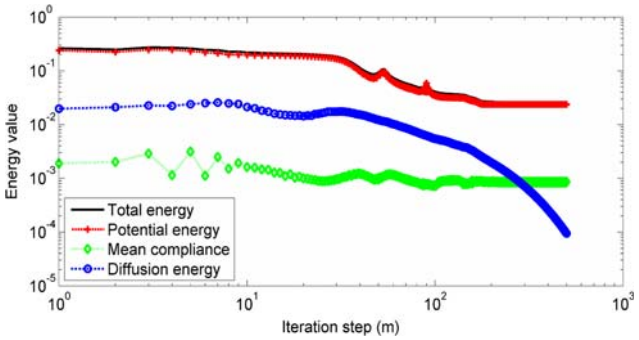

Fig. 8 The convergence of the objective function and its components

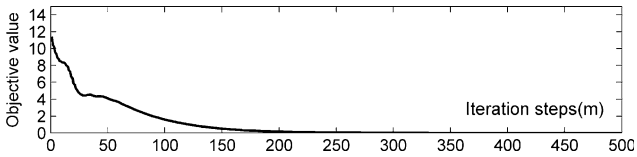

Fig. 11 Convergence of the objective function in Example 4

that the Young's modulus and volume fraction (from left to right) change gradually from 0.0094 to 0.245 and from 0.1663 to 0.3760, respectively, while the Poisson's ratio is kept at 0.89. Figure 11 plots the convergence history of the objective function given in Eq. 10. Unlike Example 3 in Fig. 9, the topologies in all the PBCs across different layers herein resemble each other. It is interesting to mention that despite the topological differences, the gradients of the volume fraction and Young's modulus are considerably similar in Examples 3 and 4 (compared to the curves in Figs. 9 and 10). Like those microstructures in bamboo section [6], it is seen that these two FGM designs in Figs. 9 and 10 have a sizeable increase in the thickness of solid materials (similarly to that in the fiber sizes of bamboo microstructure) along gradient direction.

Example 5 is presented in Fig. 12, whose microstructure is generated from Initial Design 2 for a FGM with a negative effective Poisson's ratio ($\upsilon = -0.51$) over the 12 layer-seeded GBC model. The curves in Fig. 12 illustrate the gradients of Young's modulus (from 0.0488 to 0.1827) and volume fraction (from 0.4890 to 0.7527). It is observed again that the topologies in different layers of PBCs are somewhat similar but the thickness of solid phase varies. Such a design appears in a good agreement with the report of the negative Poisson's ratio materials in [44], where

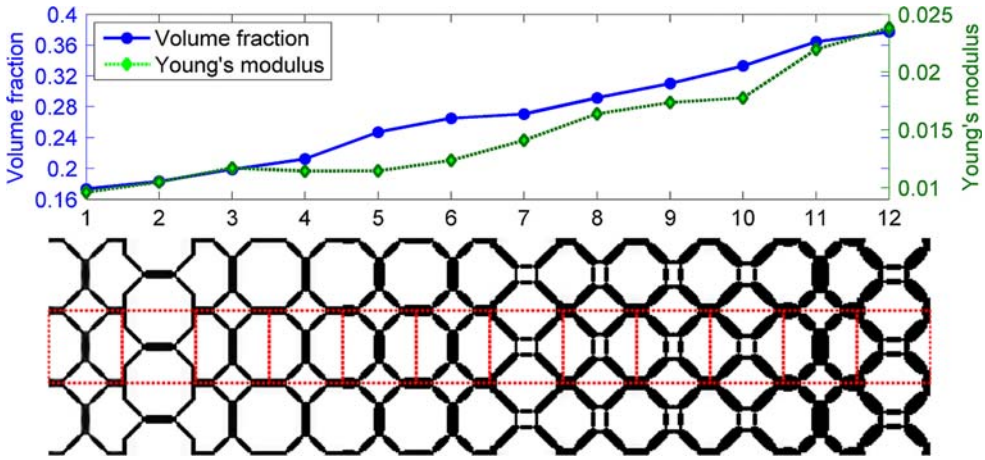

Fig. 9 FGM with a positive effective Poisson's ratio $\upsilon = 0.89$ (Example 3)

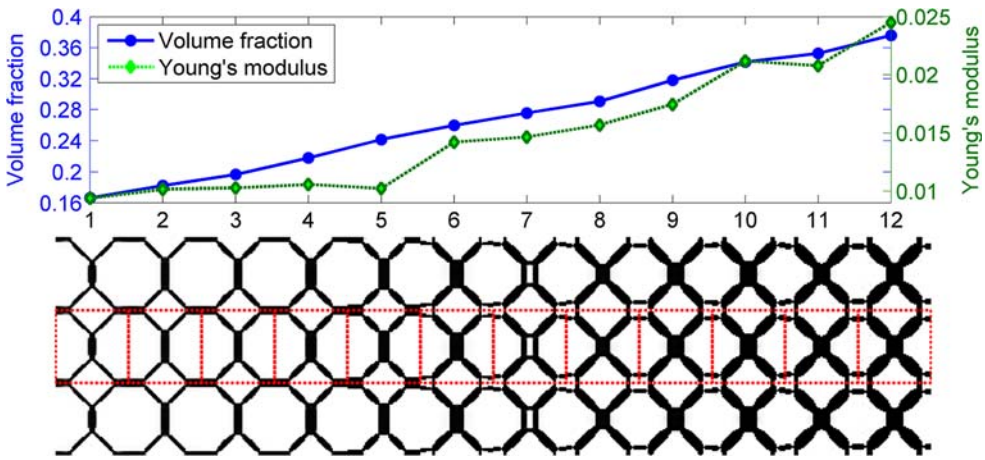

Fig. 10 FGM with a positive Poisson's ratio $\upsilon = 0.89$ (Example 4)

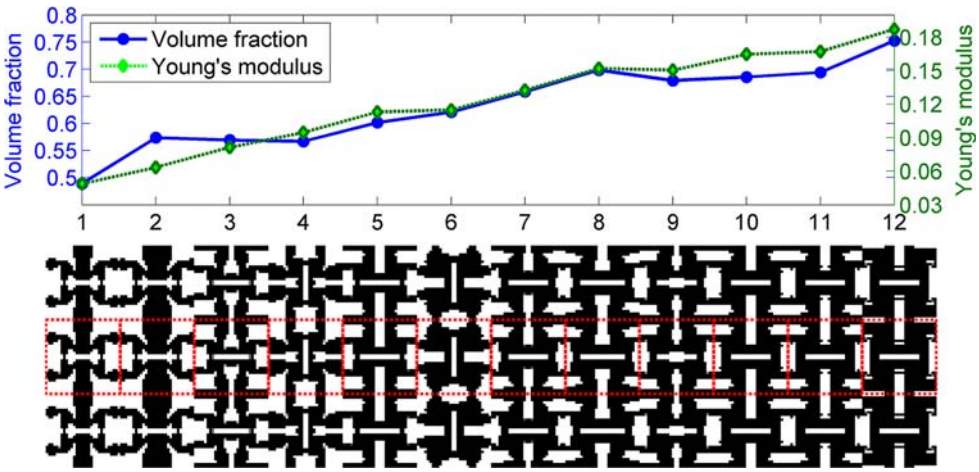

Fig. 12 FGM with negative Poisson's ratio $\upsilon = -0.51$ (Example 5)

polyethylene foams of several different cell sizes are studied on their transformation.

It is also noted that all the connectivity between the adjacent PBCs preserves well in Examples 3, 4 and 5, although there are no constraints of connective boundary and/or loads imposed for either Initial Designs 1 or 2. This demonstrates the effectiveness of such a unified formulation and the role of the nonlinear diffusion term.

Conclusion

This article presents an inverse homogenization methodology for microstructure design of FGMs. To ensure connectivity between PBCs with property gradients, three different approaches, namely (1) connective constraints, (2) pseudo load and (3) unified formulation with nonlinear diffusion, are proposed. Of them, the first two approaches design PBCs individually. In these cases, proper kinematical connective areas (in a form of non-design domain) or pseudo load and boundaries are prescribed prior to the design of each PBC model. The examples demonstrated that desirable interconnection across the PBC boundary is generated. Different from these individual PBC design methods, the third approach formulates the graded property through a GBC model with finite number of layers, where the entire FGM microstructure is designed altogether. In this scenario, three different examples with either the constant positive or negative Poisson's ratios demonstrated that the unified modeling method can effectively avoid the difficulty of prescribing connective constraints and/or pseudo loads in order to ensure PBC interconnection in the GBC model. These three approaches provide effective means to microstructural design of FGM.

It should be pointed out that although compositional FGM design could allow smoother gradients of properties theoretically, the particle and/or grain sizes may practically restrict their true continuity. The FGM microstructural design presented herein has no specific dimensional factors and can be made in any sensible scale that the current and futuristic fabrication technologies provide [17–19], which makes this present design methodology equally practical.

Acknowledgement The financial supports from Australian Research Council (Nos. DP0558497 and DP0773726) are acknowledged.

References

1. Niion M, Maeda S (1990) J Iron Steel Inst Jpn 30:699
2. Miyamoto Y (1999) Functionally graded materials: design, processing and applications. Kluwer Academic Publishers, Boston, London
3. Paul W (2001) 21st Century manufacturing. Prentice-Hall Inc., New Jersey
4. Amada S, Untao S (2001) Compos B Eng 32:449
5. Nogata F, Takahashi H (1995) Compos Eng 5:743
6. Silva ECN, Walters MC, Paulino GH (2006) J Mater Sci 41:6991. doi:10.1007/s10853-006-0232-3
7. Ray AK, Das SK, Mondal S, Ramachandrarao P (2004) J Mater Sci 39:1055. doi:10.1023/B:JMSC.0000012943.27090.8f
8. Bendsøe MP, Sigmund O (2003) Topology, optimisation: theory, methods, and applications. Springer, Berlin, New York
9. Sigmund O (1994) Int J Solids Struct 31:2313. doi:10.1016/0020-7683(94)90154-6
10. Sigmund O (1994) Design of material structures using topology optimization. Technical University of Denmark
11. Bensoussan A, Papanicolaou G, Lions JL (1978) Asymptotic analysis for periodic structures. North Holland Pub Co., Amsterdam
12. Sanchez-Palencia E (1980) Non-homogeneous media and vibration theory. Springer-Verlag, Berlin
13. Sigmund O, Torquato S (1996) Appl Phys Lett 69:3203. doi:10.1063/1.117961
14. Zhou SW, Li Q (2007) J Phys D Appl Phys 40:6083. doi:10.1088/0022-3727/40/19/048
15. Zhou SW, Li Q (2008) J Mater Res 23:798. doi:10.1557/jmr.2008.0101
16. Guest JK, Prévost JH (2007) Comput Methods Appl Mech Eng 196:1006. doi:10.1016/j.cma.2006.08.006

17. Mumtaz KA, Hopkinson N (2007) J Mater Sci 42:7647. doi:10.1007/s10853-007-1661-3
18. Dimitrov D, Schreve K, de Beer N (2006) Rapid Prototyping J 12:136. doi:10.1108/13552540610670717
19. Wang JW, Shaw LL (2006) J Am Ceram Soc 89:3285. doi:10.1111/j.1551-2916.2006.01206.x
20. Lin CY, Hsiao CC, Chen PQ, Hollister SJ (2004) Spine 29:1747. doi:10.1097/01.BRS.0000134573.14150.1A
21. Lin CY, Schek RM, Mistry AS, Shi XF, Mikos AG, Krebsbach PH et al (2005) Tissue Eng 11:1589. doi:10.1089/ten.2005.11.1589
22. Hollister SJ (2005) Nat Mater 4:518. doi:10.1038/nmat1421
23. Chen KZ, Feng XA (2004) Comput Aid Des 36:51. doi:10.1016/S0010-4485(03)00077-0
24. Zhu F, Chen KZ, Feng XA (2006) Adv Eng Software 37:20. doi:10.1016/j.advengsoft.2005.03.016
25. Seepersad CC, Kumar RS, Allen JK, Mistree F, McDowell DL (2004) J Comput Aided Mater Des 11:163. doi:10.1007/s10820-005-3167-0
26. Schramm U, Zhou M (eds) (2006) Recent developments in the commercial implementation of topology optimization. Springer, Netherlands
27. Bendsøe MP, Kikuchi N (1988) Comput Methods Appl M 71:197. doi:10.1016/0045-7825(88)90086-2
28. Sigmund O (1994) J Intell Mater Syst Struct 5:736. doi:10.1177/1045389X9400500602
29. Cheng KT, Olhoff N (1981) Int J Solids Struct 17:305. doi:10.1016/0020-7683(81)90065-2
30. Markworth AJ, Ramesh KS, Parks WP (1995) J Mater Sci 30:2183. doi:10.1007/BF01184560
31. Mori T, Tanaka K (1973) Acta Metall 21:571. doi:10.1016/0001-6160(73)90064-3
32. Hill R (1965) J Mech Phys Solids 13:213. doi:10.1016/0022-5096(65)90010-4
33. Reiter T, Dvorak GJ, Tvergaard V (1997) J Mech Phys Solids 45:1281. doi:10.1016/S0022-5096(97)00007-0
34. Hashin Z, Shtrikman S (1962) J Appl Phys 33:3125. doi:10.1063/1.1728579
35. Zhou SW, Li Q (2008) Compu Mater Sci in progress
36. Zhou M, Rozvany GIN (1991) Comput Methods Appl Mech Eng 89:309. doi:10.1016/0045-7825(91)90046-9
37. Stolpe M, Svanberg K (2001) Struct Multidiscip Optim 22:116. doi:10.1007/s001580100129
38. Bendsoe MP, Sigmund O (1999) Arch Appl Mech 69:635. doi:10.1007/s004190050248
39. Svanberg K (1987) Int J Numer Methods Eng 24:359. doi:10.1002/nme.1620240207
40. Haug EJ, Choi KK, Komkov V (1986) Design sensitivity analysis of structural systems. Academic Press, Orlando
41. Aubert G, Kornprobst P (2006) Mathematical problems in image processing: partial differential equations and the calculus of variations. Springer, New York
42. Wang MY, Zhou S, Ding H (2004) Struct Multidiscip Optim 28:262. doi:10.1007/s00158-004-0436-6
43. Bourdin B (2001) Int J Numer Methods Eng 50:2143. doi:10.1002/nme.116
44. Brandel B, Lakes RS (2001) J Mater Sci 36:5885. doi:10.1023/A:1012928726952